# CFD Modeling of Pharmaceutical Isolators with Experimental Verification of Airflow

N. NAYAN,[1] H. U. AKAY,[1,*] M. R. WALSH,[2] W. V. BELL,[2] G. L. TROYER,[2] R. E. DUKES,[2] AND P. MOHAN[2]

[1]*Computational Fluid Dynamics Laboratory, Department of Mechanical Engineering, Indiana University-Purdue University Indianapolis (IUPUI), Indianapolis, IN 46202;* [2]*Eli Lilly and Company, Indianapolis, IN 46285*

*ABSTRACT:* Computational fluid dynamics (CFD) models have been developed to predict the airflow in a transfer isolator using a commercial CFD code. In order to assess the ability of the CFD approach in predicting the flow inside an isolator, hot wire anemometry measurements and a novel experimental flow visualization technique consisting of helium-filled glycerin bubbles were used. The results obtained have been shown to agree well with the experiments and show that CFD can be used to model barrier systems and isolators with practical fidelity. This indicates that CFD can and should be used to support the design, testing, and operation of barrier systems and isolators.

*KEYWORDS:* Computational fluid dynamics, Barrier systems, Isolator, Fluid mechanics, Simulation, Parenteral, Airflow, Isolator cycle development, Pharmaceutical, Isolator decontamination

## 1 Introduction

The application of barrier systems and isolators in aseptic operations in the pharmaceutical industry has seen a significant increase in recent years (1). As a result, various aspects of designing, validating, and operating these devices have been studied by practitioners and researchers. Melgaard (2) provides a comprehensive review of the technology and its application with a focus on design issues. Nieskes (3) commented on the use of isolators for sterility testing and issues related to the load arrangement and load items.

The increased use of barrier systems and isolators comes at a time where the FDA is expecting that the design and operation of equipment and processes be underpinned by scientific and engineering rigor, focusing on mechanistic understanding rather than empirical correlations or evidence. These expectations are articulated in the *Quality by Design* and *Process Analytical Technology* initiatives (4, 5). As a result, one must begin to understand barrier systems and isolators with respect to the fluid mechanics that governs their behavior.

*Corresponding author: Tel.: +1-317-274-9710; fax: +1-317-274-9744, Email address: hakay@iupui.edu (H.U. Akay)

While the equations of fluid mechanics have been well-developed for some decades, solutions to practical problems described by these equations require computational techniques (6). Such techniques have been available at a practical level only in the last 15 years, but increasingly so in the last eight years because the computer power needed to solve such problems is now available and affordable. Computational fluid dynamics (CFD) has, thus, arisen as a science for modeling a wide variety of fluid flow applications with practical fidelity.

The use of CFD to model airflow has already been demonstrated in related applications such as the design of laboratory safety enclosures (7). The full range of applications includes those in the aerospace, chemical, and automotive industries where CFD is used regularly to predict characteristics such as flow velocity, temperature, pressure, and turbulence for compressible and incompressible, multiphase flows. A review of the applications of CFD in the pharmaceutical industry has also been published (8) with emphasis in fluid mixing, filling, solids handling, and drying. Practical advantages of CFD modeling include the ability to evaluate a variety of design alternatives without constructing prototypes, to produce an optimal design and operation protocols with limited experimentation, and to examine the flow behavior in the entire "space" of the de-

vice—something no practical amount of instrumentation could accomplish.

Application of CFD modeling to barrier systems and isolators is emerging. Melgaard (2) discusses some advantages of the use of computer modeling for ergonomic and airflow design. One of the first detailed CFD studies (9, 10) focused on modeling in two parts. First airflow patterns are computed. Next, using the predicted airflow, decontaminant dispersion and concentration are computed. This type of application is important for design and operation of isolators because the concentration of decontaminant throughout the isolator affects the overall decontamination process (11).

The objective of the present work is to build upon past efforts of those like Melgaard (2), Divelbiss and Wintner (9, 10) and to provide a basis for bringing into mainstream practice the use of CFD to predict flow patterns and distribution of air and decontaminant inside the isolator. This is accomplished by constructing a CFD model of an eight-glove transfer isolator. From this model, humid air and decontaminant flows, and decontaminant dispersion that would occur in the conditioning and decontamination phases of the biodecontamination, cycle are computed. The computed flow results are experimentally verified. Gas flow is measured using hot wire anemometry and a novel experimental flow visualization technique consisting of helium-filled glycerin bubbles. The bubble technique differs from traditional smoke tests and ensures relatively greater accuracy. The use and limitations of these measurement systems are presented along with model construction details and a comparison of predicted and measured results.

The nature of construction of the CFD model and the large body of supporting experimental data produced by this work provide a basis for constructing models of many types of barrier systems and isolators to support their design, cycle development, and validation. Incorporating CFD models in these activities will lead to improved system design, efficient validation protocols, and shorter decontamination cycles. Further, the CFD models provide a scientifically rigorous basis from which the design, testing, and operation protocol of barrier systems and isolators arise.

## 2 Governing Equations

CFD is a technology by which one obtains numerical solutions to the equations governing the behavior of fluids. These governing equations arise from the basic conservation laws of physics: conservation of mass, conservation of momentum, and conservation of energy. The completely general equations take specific forms based on the particular attributes of the flow being modeled. The flow in an isolator is a case of compressible, turbulent, isothermal (because this case is isothermal, the equations arising from the conservation of energy need not be included in this model) flow of a Newtonian fluid. For such a case the equation for conservation of mass can be written as:

$$\frac{\partial \rho}{\partial t} + \nabla \cdot (\rho \vec{v}) = S_m \qquad (1)$$

The operator $\nabla$ represents the three-dimensional vector differential (gradient) operator, $\rho$ is the density, $\vec{v}$ is the velocity vector, and $t$ is time. The source term, $S_m$, represents the mass added to the system such as mass inlet at boundaries and mass generated by reactions.

Conservation of momentum arises from Newton's Second Law and in an inertial (non-accelerating) reference frame can be expressed as

$$\frac{\partial}{\partial t}(\rho \vec{v}) + \nabla \cdot (\rho \vec{v}\vec{v}) = -\nabla p + \nabla \cdot (\bar{\bar{\tau}}) + \rho \vec{g} + \vec{F} \qquad (2)$$

where $p$ is the static pressure, $\bar{\bar{\tau}}$ is the stress tensor as defined below, $\rho \vec{g}$ is gravitational body forces, and $\vec{F}$ contains other model-dependent momentum source terms such as porous-media effects in filters. For a Newtonian fluid, the stress tensor $\bar{\bar{\tau}}$ is related to velocity by Newton's Law of Viscosity. Using that relation the stress tensor becomes

$$\bar{\bar{\tau}} = \mu[(\nabla \vec{v} + \nabla \vec{v}^T) - 2/3(\nabla \cdot \vec{v})\bar{\bar{\delta}}] \qquad (3)$$

where $\mu$ is the molecular viscosity, $\bar{\bar{\delta}}$ is the unit tensor, and the second term on the right hand side is the effect of volume dilation. Combination of eqs 2 and 3 give the familiar Navier-Stokes equation. Complete development of these equations is presented in several texts on fluid mechanics (12, 13).

As the Reynolds number based on the gas inlet ranged from 200 to 2000, the flow was either laminar or low transitional. Transitional regimes are the intermediate regime between laminar and turbulent and therefore

can be considered as composites of laminar and turbulent regimes. In order to correctly simulate the turbulence, models with sub-millimeter-scale flow structures are needed. As a general rule, this is not practical with the current computing technology. Consequently, expressions of velocity and pressure based on Reynold's averaging are used in the Navier-Stokes equations; see Johnson (13). When these substitutions are made, the Reynolds Averaged Navier Stokes (RANS) equations result. In these equations the momentum balance becomes

$$\frac{\partial}{\partial t}(\rho\vec{v}) + \nabla \cdot (\rho\vec{v}\vec{v}) = -\nabla p + \nabla \cdot (\bar{\bar{\tau}}) + \rho\vec{g} + \vec{F} + \nabla \cdot \bar{\bar{\tau}}' \quad (4)$$

which now contains the additional term

$$\bar{\bar{\tau}}' = \rho\overline{\vec{u}\vec{u}} \quad (5)$$

This term is called the Reynold's stress tensor. In this term, $\vec{u}$ is the fluctuating component of velocity as defined by Reynold's averaging. Solutions to the RANS equations are possible when a connection is made between the Reynold's stress tensor and the mean velocity field. The development of models for making this connection is described by Johnson (13) and has resulted in a class of so-called two-equation models that have successfully modeled turbulent flow for several classes of flow conditions. Because of the nature of the flow in this work, the K-ω model was used to model turbulence (14, 15). The details of this method are based on the work of Wilcox (16). In this model, as in most of the two-equation models, the Reynold's stress tensor is related to the mean velocity through an eddy viscosity. The eddy viscosity is cast as a function of K, the isotropic turbulent kinetic energy, and ω, the specific dissipation rate of K into heat by molecular friction. These terms are computed from transport equations similar in form to eq 2. From these results the eddy viscosity is determined and used to relate the Reynold's stress tensor to average velocity through the Boussinesq hypothesis (17).

These equations, along with the initial and boundary conditions described below, are solved numerically using a finite volume construction and an implicit, segregated, discretization of the governing equations as implemented in the commercial (CFD) code Fluent v6.2.16 (18). From the solution, the velocity vector field and the pressure distribution are generated. An extensive collection of references exists that describe the details of these discretization and solution methods. The texts by Ferziger and Peric (19) and by Anderson (20) are among them.

## 3 CFD Model of the Isolator

The stages of bio-decontamination for the isolator in this study can be listed as (21, 22):

Phase 1: Dehumidification. This is the primary phase in the isolator chamber where conditions are created for decontamination.

Phase 2: Conditioning. In this phase, concentration of decontaminant is raised rapidly to effective levels using high decontaminant supply rates.

Phase 3: Decontamination. In this phase, decontaminant supply rate is maintained at a level suitable for maintaining the desired concentration for decontamination. In this phase the decontaminant supply rate is typically lower than that in the Conditioning phase.

Phase 4: Aeration. In aeration, the decontaminant is purged by using either the generator or the facility venting system to reduce the concentration to a value below which operations may be safely resumed.

The focus of this work is on flow conditions that are present during conditioning or decontamination phases, and on isolators that use vapor phase hydrogen peroxide (VPHP) as the decontaminant (23). Under these conditions the operating temperature changes are small enough that physical properties change very little. Therefore, the simulations were performed under isothermal conditions.

A CFD analysis on isolators performed here consisted of four main steps:

First, a three-dimensional geometric model of the isolator and its components, such as interior objects, gloves, and fans, is created. The gloves are modeled as cylindrical shapes protruding inside or outside the isolator.

Second, after the creation of the isolator geometry, the entire space is divided into hundreds of thousands of connected geometric elements, or cells, that form a grid or computational mesh. This *mesh generation* step is important because the nature of the element

**TABLE I**
**Conditions Modeled Using CFD**

| Supply Velocity (m/s) | Fluid | Glove Position | RTP Sleeve | Internal Fans Operating? | Remarks |
|---|---|---|---|---|---|
| 0.1 | Air | In/Out | Extended/Absent | Yes/No | Investigated using CFD and helium bubble generator |
| 0.45 (actual experimental case) | Air | In/Out | Extended/Absent | Yes/No | Investigated using CFD and hot wire anemometry |

shapes, their size, and the way they are connected can affect the computational characteristics of the solution such as convergence (18, 19).

Third, this mesh is loaded into a numerical processor. The numerical processor used in this work was Fluent™ v6.2.16 (18). Inputs, such as the fluid properties, and boundary conditions, such as inlet flow rates and fan flow rates, are specified. The numerical processor solves the mass, momentum, and turbulence balance equations presented above for each cell for six unknowns—pressure (p), three velocity components ($u_x$, $u_y$, $u_z$), and two turbulence values (turbulent kinetic energy (K) and specific dissipation ($\omega$).

The last step in the process is called post-processing. This is where the results are displayed and analyzed.

The fluid velocity vectors and the pressure distribution inside the isolator are the key results obtained using CFD to model the isolator. The cases investigated in this study using the CFD method are enumerated below. In all cases, the pressure at the gas outlet was specified as 1 atm.

Case 1—Airflow in the presence of internal mixing fans at 0.45 m/s supply velocity.

Case 2—Airflow in the absence of internal fans at 0.1 m/s supply velocity.

Case 3—Airflow in the absence of internal fans at 0.45 m/s supply velocity.

Case 4—Airflow in the absence of gloves and internal mixing fans with obstructions at 0.1 m/s.

Case 5—Airflows in the presence of a rapid transfer port (RTP) sleeve with and without gloves at 0.45 m/s with mixing fans.

Placement of objects inside the isolator was simulated (Case 4) because such objects can affect the flow patterns. The specific placement of objects inside the isolator was made with some guidance from previously used set-ups (24). Because of computational limitations in modeling the details of the supply and return HEPA filters, uniform boundary conditions were specified for both. At the inlet a fixed velocity was specified, and at the outlet the pressure was specified.

Models were constructed representing the absence of gloves and the inward extension of the gloves both with the presence of the RTP sleeve (Case 5). The RTP was omitted in the initial case studies partly because the reports published in past have indicated that the RTP can be omitted in many cases if the isolator is constructed with rigid walls (25). We found this is not necessarily the case.

After obtaining the CFD predictions of the airflow in either conditioning or decontamination phases, velocity profiles visualizations were produced for sections inside the isolator in order to investigate areas of reduced or no flow. These results were compared with those obtained using a hot wire anemometer (26) and with the helium bubble generator (27), wherever possible. The flow and the fluid conditions are highlighted in Table I.

The geometric model of the eight-glove isolator in the standard configuration with gloves extended inward and the RTP sleeve is shown Figure 1. Other configurations that were investigated but not pictured here were the inclusion of internal mixing fans and the presence of interior objects. The computational mesh was composed of 410,000 ± tetrahedral cells in cases without the RTP sleeve, but with additional cells when the RTP sleeve was included. Cells were more densely packed in areas where more detail was needed or gradients were expected to be large. The number of

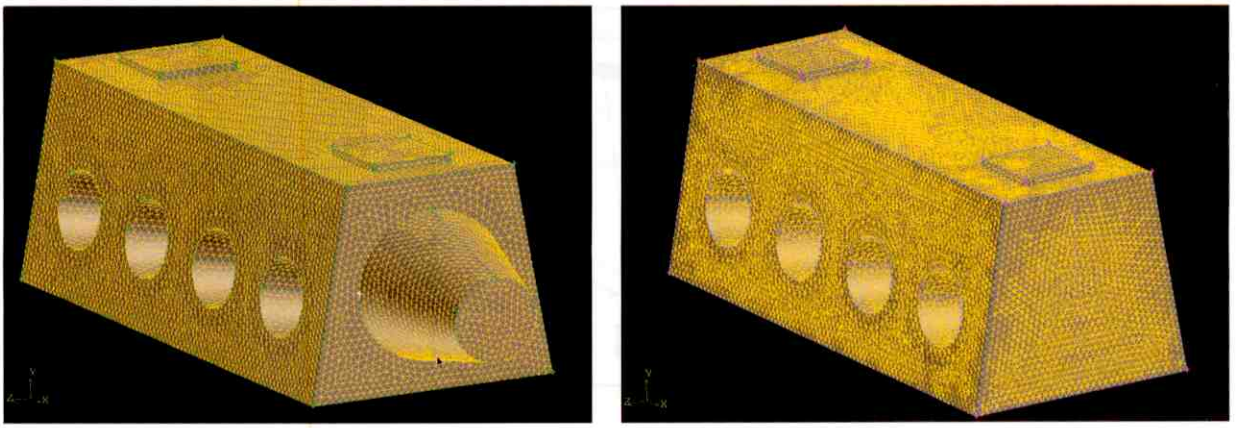

(a) (b)

**Figure 1**

**CFD model of the transfer isolator: (a) gloves inserted and RTP sleeve extended, and (b) without RTP sleeve.**

cells used in this study is considerably larger than any simulation that has been carried out in previously published research on modeling isolators. Using a larger number of cells has ensured a more accurate prediction as shown by the convergence study undertaken (see results and Figure 7). Typically, the total time for reaching a converged steady state solution in such simulations was between 11 and 12 hours of wall-clock time on Linux clusters with 2.5 GB RAM and 2.4 GHz Pentium 4 Xeons. In some instances, parallel processing was also used for faster simulation time, and a marked improvement was observed in the turn-around time.

Simulation results are assessed based on numerical considerations and physical realization. This includes monitoring the progression of scaled residuals, which indicates degree of convergence, and checking the overall mass balance and pressure balance, which indicate a physically realizable solution.

## 4 Experimental Methods for Verification of CFD Models

The transfer isolator unit consisted of eight gloves and a RTP attached to a flexible/collapsible polymer sleeve, which was attached to one end of the isolator. The isolator is accessible to the operator for introduction of material by the use of a hatched door on one side and through the RTP on the other. The supply and the return in this Class 100 (ISO 5) system are located at the top where high-efficiency particulate air (HEPA) filters are fitted for preserving the isolator's integrity (28). This arrangement provides the isolator with non-unidirectional flow. In order to enhance the mixing, the isolator is equipped with two internal mixing fans, one near the supply and the other near the return. The construction material used is 316L stainless steel, glass, and polyurethane. This geometry of a transfer isolator is typical of those used in pharmaceutical industries worldwide. Figure 2 shows a graphic representation of the eight-glove isolator without the RTP sleeve.

### *4.1 Hot Wire Anemometry*

In order to conduct velocity measurements, two approaches were used. In the first approach, a hot wire anemometer (26) was used to conduct point measurements. For these measurements a Kanomax Climomaster Model A531 with a Model A533-01 probe was used. The image in Figure 3 shows the equipment and

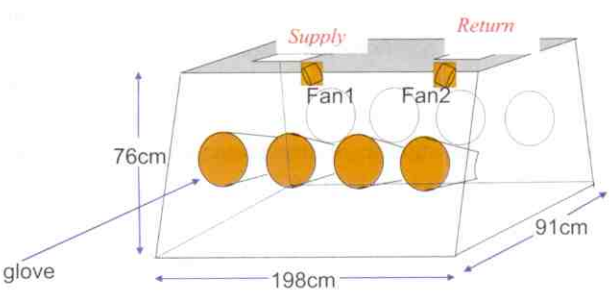


**Figure 2**

**Sketch of the eight-glove transfer isolator.**

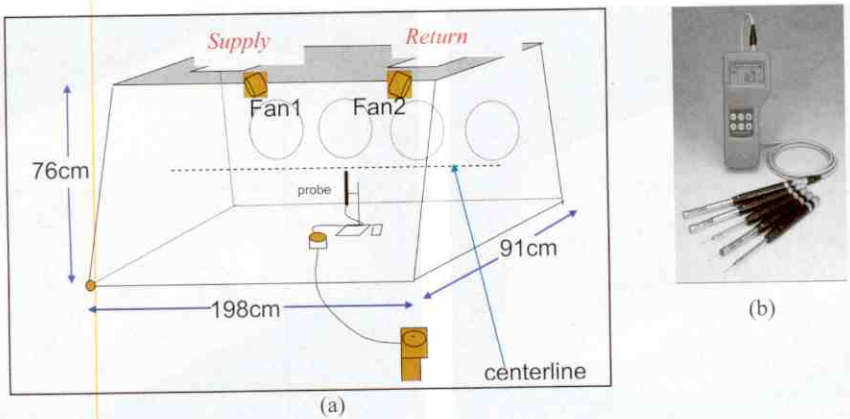


**Figure 3**

**(a) The set-up of the Kanomax probe and unit inside isolator, and (b) the Kanomax device.**

its positioning inside the isolator. The velocities were obtained in the geometric center as indicated in the same figure. This device provides the most accurate measurement of flows that are perpendicular to the probe. A low response will be obtained for flows that are at angles of approximately $<45^{\circ}$ or $>135^{\circ}$ to the probe. The device was capable of measuring velocities from 5 m/s to 0.05 m/s with a published accuracy of 3% of the reading +0.1 m/s. The accuracy of this device is typical of anemometer-type measurements and is poor in the low-flow regime typical of isolator use. CFD model Cases 1, 3, and 5 were developed so that a comparison of model and measurement could be made in a flow regime where the measurements were reasonably accurate.

During measurements, the probes were held in place using a ring stand and clamp to avoid measurement errors associated with shaking or other movement that could result when holding the probe by hand. In the figure, the probe is positioned vertically to register the component of the flow accurately in bulk of the isolator domain because these flows were expected to be primarily in a horizontal direction. However, for measurements beneath the supply, the flow was mainly downwards and the probe was positioned horizontally to capture these velocities accurately. This technique has certain limitations when applied to low-velocity fields such as indoor flows (29), and significant measurement errors have been reported for flows up to 0.25 m/s.

*4.2 Helium Bubble Generator Technique (Particle Tracking Velocimetry)*

The other method used for obtaining velocities works on a similar principle to laser based velocimetry such as particle image velocimetry (PIV) or laser doppler velocimetry (LDV) (8, 30). However, this was a much more inexpensive approach and is capable of being used in vapor rather than liquid media. The technique provides flow visualization comparable in principle to the laser-based velocimetry, and it presented the advantage of being able to be configured in a laboratory environment. A Sage Action, Inc. model 5 helium bubble generator (Figure 4) was used to produce helium-filled bubbles inside the isolator. The diameter of the bubbles could be varied from 1/32″ to 3/16″ and, as part of the set-up, the bubble sizes were adjusted so that they were at or near neutral buoyancy. The bubble generator was located outside the isolator and the bubbles were transferred into the isolator through a piece of Tygon® tubing (Figure 6). At the end of this tubing were two Y-connectors so that bubbles could be released from several different points. As the bubbles followed air movement, their displacement was recorded by a Redlake Motion Scope High Speed Video Unit camera (512 X 512 pixels) recording at 60 frames per second. The camera signal was recorded on VHS tape using a Panasonic AG-1980 SVHS videocasette recorder. Because the camera could only capture motion in two dimensions, it was necessary to limit the detection of bubbles to a known location in the third dimension. This was accomplished with a strip light source consisting of a high-intensity Fostec DCR II Light Unit coupled to a 10-inch Fostec Microfiber bar that was mounted in a cardboard box which had a ¼-inch wide by 12-inch-long slit cut into the top. This provided a narrow beam that approximated a plane of light. Bubbles outside the plane were not illuminated and were generally not visible. Bubbles inside the plane were highly visible and easy to track with the

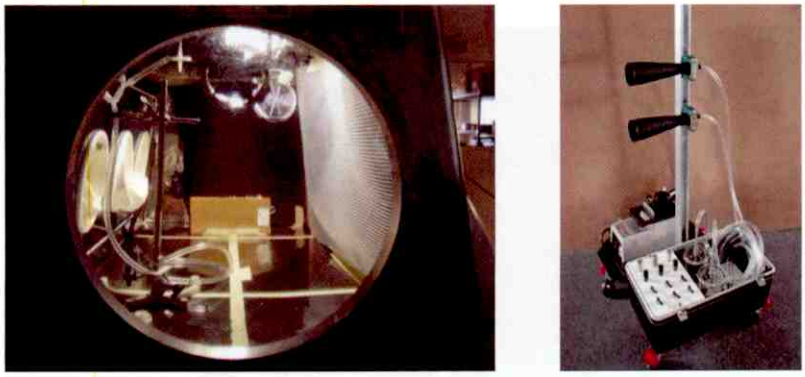

(a) (b)

**Figure 4**

**(a) Camera view from the side of the isolator, slit projection of light shown with bubble release pipe mounted on ring stand, and (b) helium bubble generator unit.**

captured video. The light source was moved to various locations to gather measurements from other portions of the isolator. To measure motion in the third dimension, the camera and light source were relocated to a position 90 degrees from the original location. Video recording from the front of the isolator was accomplished through the glass wall of the isolator, and recording from the side was accomplished through a window created by removing the RTP sleeve and covering the hole with a clear plastic film. The back and the other side wall were covered in black felt to provide maximum contrast.

The VHS-recorded video images were digitized using Pinnacle Studio™ software with an AVDV video capture card. The digitized video was analyzed using Videopoint™ software from Lenox Softworks. The Videopoint™ software enables the user to mark bubble position from frame to frame, and the software can automatically calculate position and velocity from the marked positions, as there is a known time increment between frames. Calibration of the pixel position to inches was accomplished using the dimensions of other items in the video as a reference. Figure 16 shows a screen capture from Videopoint™ showing

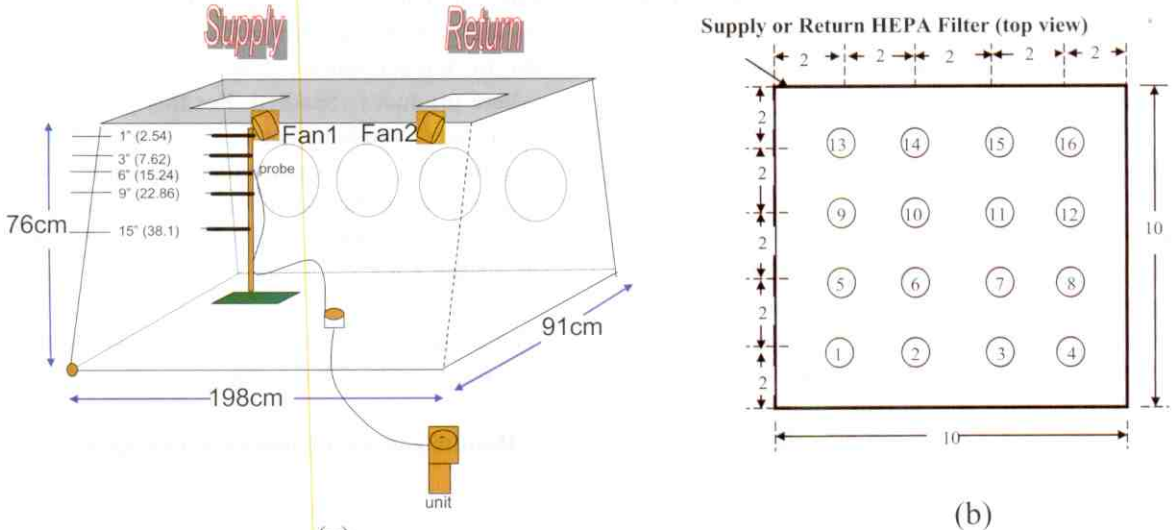


**Figure 5**

**(a) The arrangement of the probe at different levels below filter, and (b) magnified top view of the supply filter with the measurement locations and distances (units in inches).**

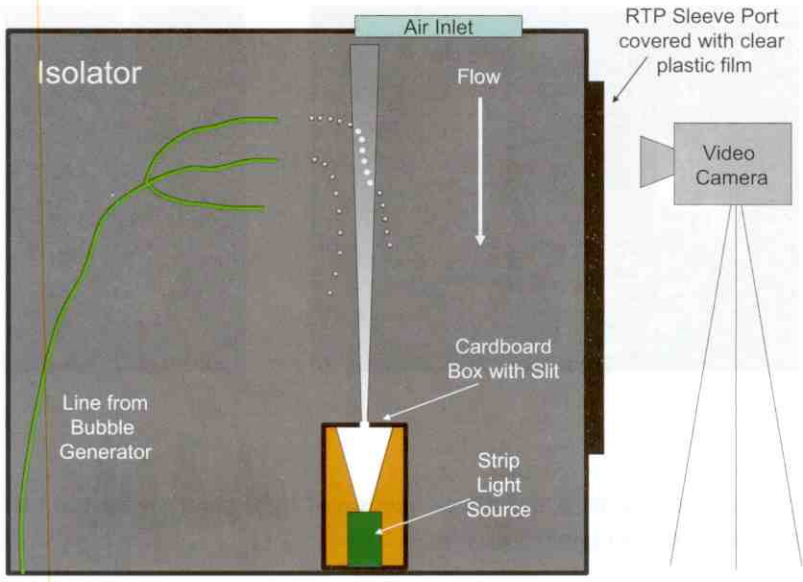


**Figure 6**

**Arrangement of camera, bubble generator, and lighting in the isolator.**

the tracks of various bubbles. By collecting data from multiple bubble tracks, one could gather velocity information at different locations and convert to flow rate. The life of bubbles was about 1–2 minutes, more than sufficient for capturing the position of the bubble with the camera.

The primary advantage of this method is that it can be used to obtain quantitative component velocity data in a plane, as well as flow visualization. This data can be compared directly with the CFD-generated vector plots using visualization software such as Tecplot™ from Tecplot, Inc.

*4.3 Supply and Return Filter Velocity Measurement*

In order to assess the uniformity of the flow from the filter, the velocity close to the filters and in the bulk flow region was obtained using the hot wire anemometer. The advantages of this exercise were that the assumption of a uniform velocity specification over the whole supply filter area in CFD simulations could be verified, the performance of the filter could be evaluated, and, if any non-uniformity existed, its effect in the center and corners of the isolator could also be examined. The method for conducting the measurements was similar to the velocity measurements in the centerline and differed only in the way the measurement location was mapped. The supply and the outlet filters were square-shaped, 10 inches on a side, and were divided into a four-by-four grid resulting in a total of 16 measurement locations. This approach is the same as that used for the measurement of flow rates from filters in the heating, ventilation and cooling (HVAC) industry (28). The only limitation of this method was that the internal mixing fans had to be kept switched off because measurement difficulties arise when a high degree of turbulence is generated.

One element of this study was to examine the flow behavior as the gas stream leaves the filter and flows to the work level, that is, close to the areas of the isolator where product is handled. For this purpose, measurements were conducted at 1, 3, 6, 9, and 15 inches from the filter face with particular attention given to the uniformity of the flow. For the purposes of clarity, only measurements at 1, 3, 6, and 15 inches are discussed here.

These measurements were carried out at the supply and return ends of the isolator as indicated in Figure 5.

## 5 Results and Comparisons with Experiments

*5.1 Velocity at the Center*

The velocity measurements were conducted using the Kanomax hot wire anemometer. During initial experiments it was found that the velocities were lower than the anemometer detection limit in most of the isolator

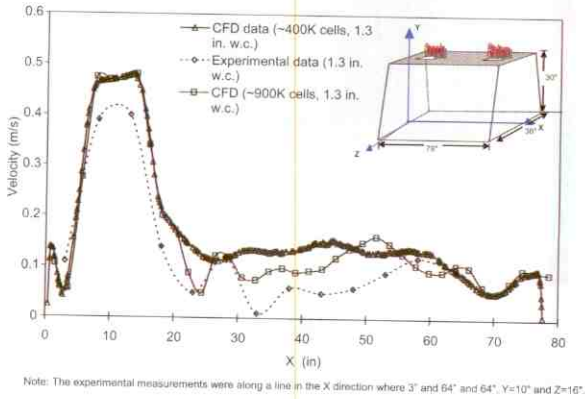


(a)

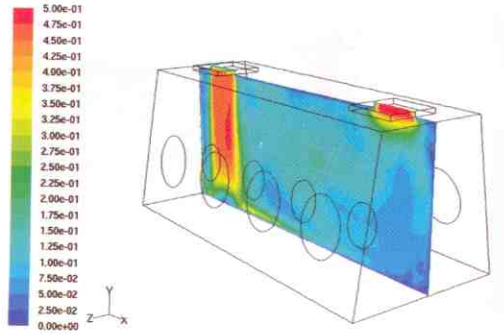

(b)

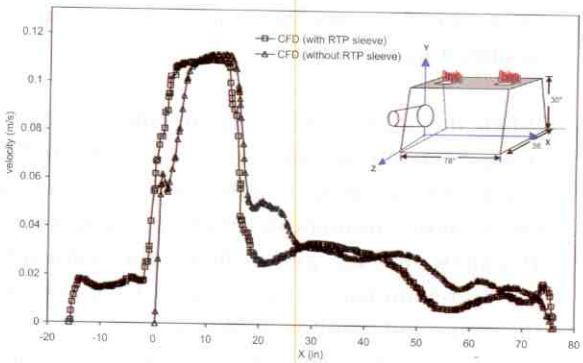


(c)

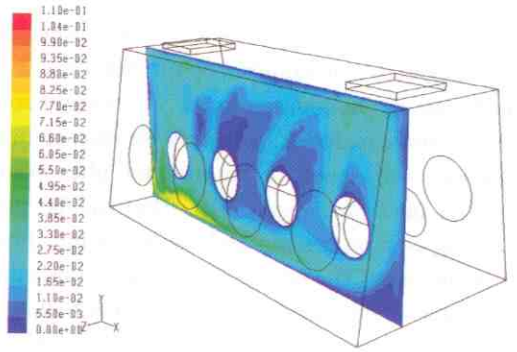

(d)

**Figure 7**

**Velocity measured: (a) using hot wire anemometer, (b) compared with CFD visualization at 0.45 m/s supply velocity at center, (c) 0.1 m/s supply velocity at center, and (d) near gloves.**

when operating the fan at normal speed (pressure equal to 0.2 inches of water). Therefore, for some of the experiments, the isolator was operated at 1.3 inches of water positive pressure, which resulted in higher flow rate of 0.45 m/s (60 $ft^3$/min) (Figure 7). For isolator pressures of 0.2 inches of water, only the velocities at a location below the supply were measurable, while the rest of the isolator had undetectable velocities. This is consistent with the error limits at the low end of the measurement range. The experimental results presented deal with cases where the measurements were the most accurate. The gloves being inside the isolator or protruding outside did not affect the velocities and flow patterns in the center but had an effect near the gloves. Velocity contours provided in Figure 7 confirmed that this was indeed the case in the absence of mixing fans. The measurements also assisted in specifying the boundary conditions for the CFD simulations.

The measurements indicated that the velocities below the supply filter were much higher than in the center (Figure 7). In such cases, where the mixing fans were not operated, large velocity gradients exist within the isolator, creating extremes of low and high flow. Low flows exist mainly in corners, and in the vicinity of the gloves, and would be even lower at lower differential pressure. The CFD simulations in the same region (i.e., the centerline of the isolator, Figure 7a) predicted slightly higher velocities than the anemometer measurement, but given that the hot wire anemometer does not measure total velocity, and the measurement error is higher at these velocities, reasonable agreement is seen.

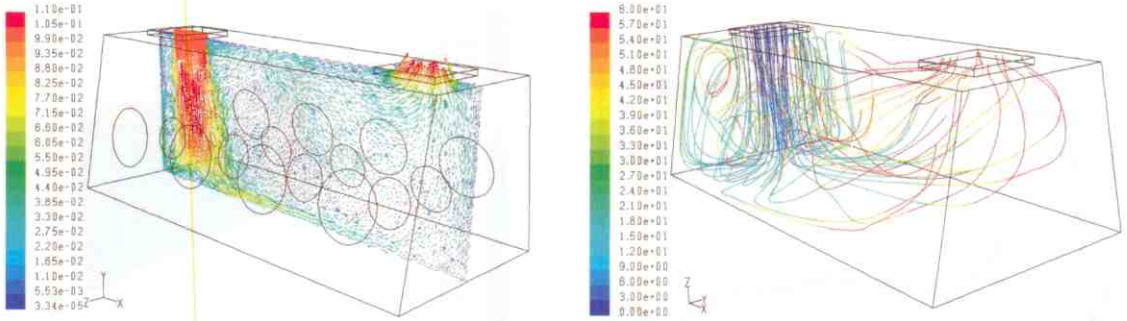

(a) (b)

**Figure 8**

**Vectors representing velocity and particle tracks in time colored by (a) velocity magnitude, and (b) time.**

Plotting the vectors is a graphical way to represent the computed velocities. An example of this for Case 2 is shown in Figure 8a. In addition to the vectors and contours, CFD is also capable of indicating the elapsed time that a particle will spend in the isolator after being released from inlet (see Figure 8b). This can be performed during post-processing and facilitates the simulation of smoke tests. The release of particles from a line across the inlet is simulated. A uniform distribution is assumed. In the figure, some particles are tracked for around 60 s. This can be used to evaluate the design without extensive experiments. Another capability of the CFD model was the ability to predict the effect of interior objects on the velocity and subsequently on the overall flow pattern, as shown in Figure 9.

This was important when the mixing fans were switched off, as proper mixing could not be guaranteed. Thus, the areas behind racks and stands could be areas difficult to decontaminate, and these areas can be identified using CFD.

When the RTP sleeve was included in the model (Case 5), two configurations were simulated to represent the operating conditions that might exist in the isolator. Simulation results presented in Figure 10a show that the gloves protruding outwards during decontamination did not affect the velocities in the center but resulted in almost zero velocity in the corner near the outlet because of slight short-circuiting of the flow. Stagnation in the flow was also found in the RTP sleeve and the gloves, as seen in Figure 10a.

The presence of HEPA filters was not modeled in these simulations because of the extra computational

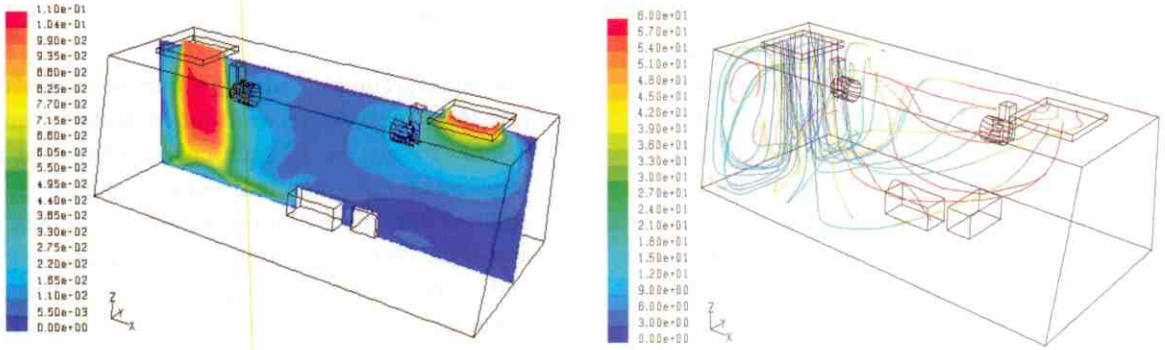

(a) (b)

**Figure 9**

**Presence of objects simulated with particle tracks: (a) velocity contours (meter/second), and (b) particle tracks colored in time.**

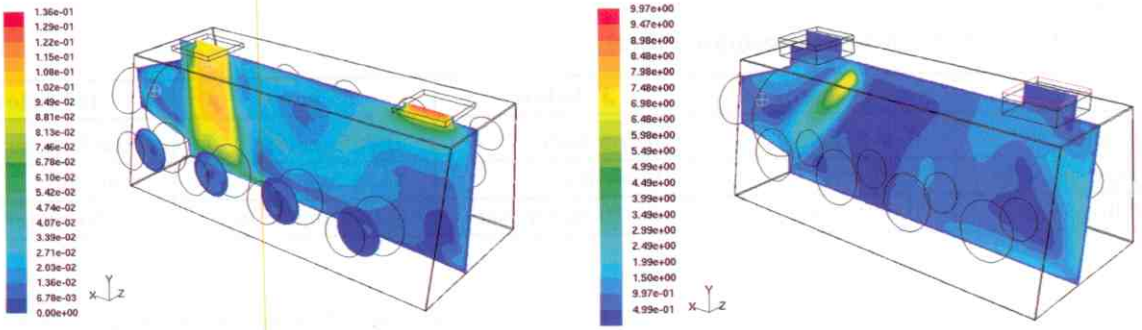


(a) (b)

**Figure 10**

**Flow with the gloves outside and RTP sleeve: (a) mixing fans off, and (b) mixing fans operating.**

time that would have been required. From the results obtained in the absence of internal mixing fans, it is possible to understand the importance of fans on providing improved mixing, especially when the air supply velocity is relatively low, as it is in this work. Hence the model was modified to include fans that were located as dictated by the actual geometry (Figure 10b) with pressure boundary conditions applied as a 100 Pa rise in pressure at the outlet faces of the fans. The fans directed flow towards the end walls of the isolator to provide recirculating flow that provided improved mixing.

In this configuration, the velocities were measured again with the hot wire anemometer. Results in comparison with CFD are presented in Figure 11. Higher velocities than those at the center were recorded near the end walls, and an overall increase in the flow velocities was noticed. Because of the nature of the measurement technique of the thermal anemometer, as explained earlier, the probe positioning was adjusted from horizontal below the filter to vertical while away from it in order to capture the x-component of the flow when the fans were not in operation. However, in cases where mixing fans were used as in Figure 11, the manipulation of the probe was not feasible because of the turbulent mixing induced by the fans. For an accurate comparison, the x-component of the velocity predicted by CFD showed a good comparison with the experimental measurement close to the walls. The agreement away from the walls is not as good because of the weak ability of the probe to resolve all velocity vector components.

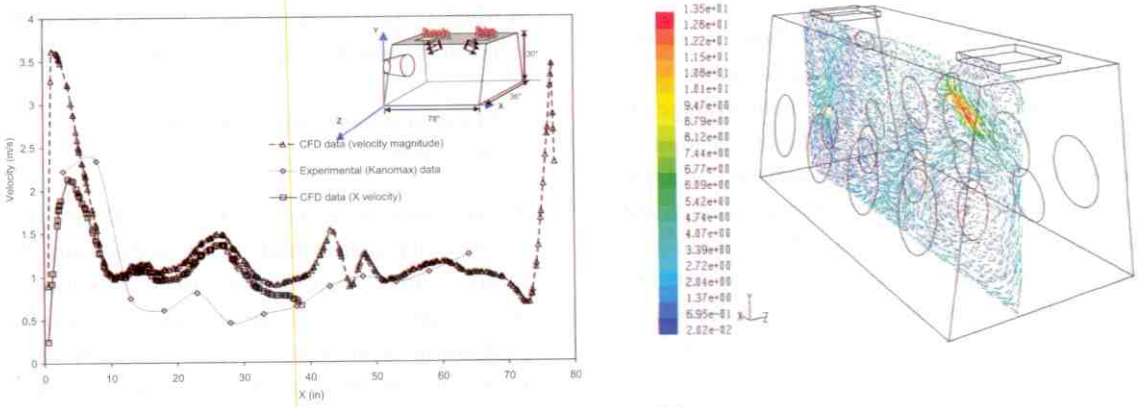


(a) (b)

**Figure 11**

**Velocity with mixing fans in operation: (a) experimental, and (b) CFD vector plot with gloves inside.**

**TABLE II**
**Velocities and Flow Rates below the Supply Filter**

| | 1″ below | 3″ below | 6″ below | 15″ below |
|---|---|---|---|---|
| Filter area | 0.065 meter$^2$ | 0.065 meter$^2$ | 0.065 meter$^2$ | 0.065 meter$^2$ |
| Average velocity | 0.45 m/s | 0.46 m/s | 0.44 m/s | 0.40 m/s |
| Duct flow rate | 0.029 meter$^3$/sec | 0.030 meter$^3$/sec | 0.029 meter$^3$/sec | 0.026 meter$^3$/sec |

*5.2 Effect of Finer Mesh*

A study was conducted to understand the effect of finer mesh on the accuracy of results. This provided an estimation of the accuracy of the simulation and also indicated if using a finer mesh produced calculated velocities that compared better with the measurements. As evident from centerline velocity plot in Figure 7a, the effect of increasing the mesh density to more than twice the original (900,000±) number of cells did not result in any significant overall improvement in the prediction of velocities below the supply filter. Further, the denser mesh model took longer to converge and its size made it less portable to other computer platforms. Consequently, additional cases were executed with the smaller (410,000±) mesh.

*5.3 Flows below the Filter*

The modeling of the flow from the supply duct was done assuming that the flow was uniform. Though this was not thought to affect the results greatly, it was necessary to conduct tests to prove the validity of the assumption. The isolator was operated at 1.3 inches of water and an explanation of the method of measurement is provided in the experimental methods section.

The measured velocity below the filter (Table II, Figure 12) showed similar values at almost all locations sampled, but was much higher at point 3 than average. If ignored, this could have an effect on the distribution of the gas-vapor. After noticing this phenomenon, the areas above the filter casing were investigated physically and the location of the supply pipe was noted (Figure 13). The placement of the supply pipe over point 3 resulted in the higher velocities at that location. As a correction to this, a flow conditioner could be placed to provide uniform velocities. In such an event, this method of sampling locations below the filter could be used for quantification of the non-uniformity of the flow.

Similar measurements near the return filter indicated the velocities to be lower than that obtained near the supply at 6 inches and 15 inches below the filter (Table III and Figure 14). This is because flow enters the return from all directions compared to the supply, which has a fan forcing the air/VPHP mixture downward through it. Additionally, there is some effect because the probe is not perfectly aligned with the direction of the bulk flow.

When the mixing fans were in operation, the effect of the non-uniformity on flow in the bulk of the isolator was mitigated and the model was developed using a uniform velocity inlet condition to avoid excessive computational time. However, our experiences have shown that in cases where the mixing fans are not operated, the inlet condition has a more pronounced effect on the flow in the bulk of the isolator, and the CFD model should include filters that provide anisotropic resistances.

On examining the CFD velocity predictions near the return, the flow directions were found to be aligned with the probe. This might have resulted in the lower velocities that were measured.

This is one indication of how boundary condition specification can affect the simulation results and confirms that the specification of boundary conditions should be guided by physical arguments or direct experimentation. Enhancements to the models described in this work include porous media boundary conditions and the eccentric location of the inlet pipe.

*5.4 Computational and Experimental Flow Visualization*

A major benefit of using CFD is its ability to compute the velocity vector field. These vectors and their magnitudes can be used to assess the distribution of VPHP that is introduced into the isolator. Experimentally, the evaluation of airflow of isolators is carried out using traditional methods such as smoke tests. The advantage of using the helium bubble generator mentioned above was twofold. First, the velocities obtained could be shown as vectors for a direct comparison with CFD predictions, and second, they could be tracked for a quantification of the velocity.

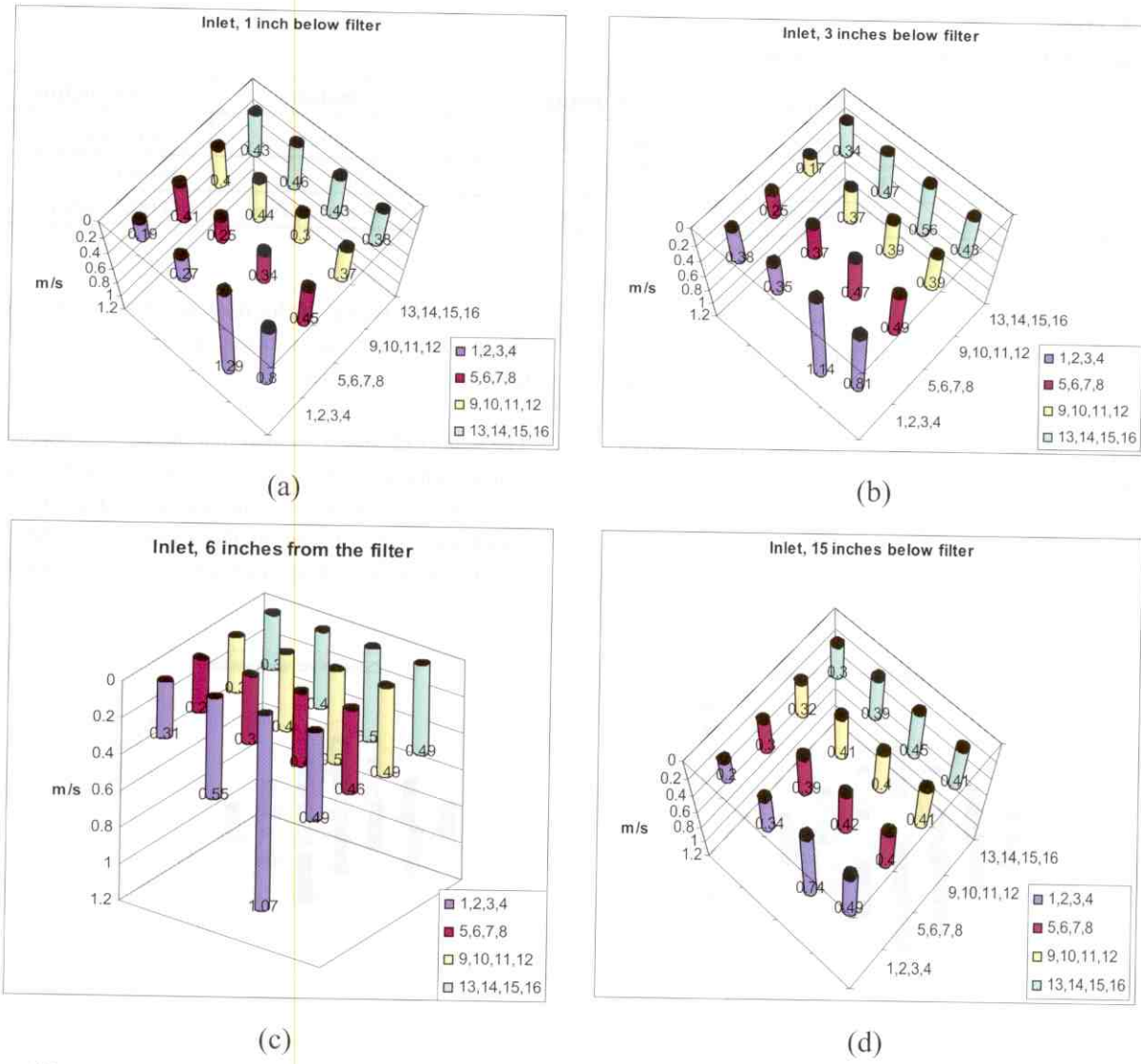


**Figure 12**

**Velocities below the supply filter at various levels: (a) 1 inch below, (b) 3 inches below, (c) 6 inches below, and (d) 15 inches below.**

The plane in which the bubbles were illuminated and the tracking procedure in time are shown in Figure 16. Data were collected at 0.2 and 1.3 inches of water differential pressure but only without the RTP sleeve and with gloves not present. Because of the arrangements of the video capturing system, an extensive analysis of all positions was not possible.

Good agreement between the CFD predictions was seen at the higher differential pressure (Figure 17). The bubble-track data compared well with CFD predictions in both direction and magnitude. Because the accuracy of this method is dependant on the number of bubble tracks that can be averaged, comparisons with

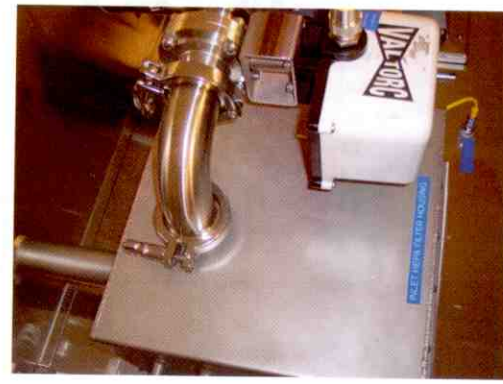

**Figure 13**

**Positioning of the supply pipe.**

**TABLE III**
**Velocities and Flow Rates below the Return Filter**

| | 1″ below | 3″ below | 6″ below | 15″ below |
|---|---|---|---|---|
| Filter area | 0.065 meter$^2$ | 0.065 meter$^2$ | 0.065 meter$^2$ | 0.065 meter$^2$ |
| Average velocity | 0.36 m/s | 0.26 m/s | 0.14 m/s | 0.046 m/s |
| Duct flow rate | 0.02 meter$^3$/sec | 0.018 meter$^3$/sec | 0.009 meter$^3$/sec | 0.003 meter$^3$/sec |

CFD results at the low pressure were inconclusive because an insufficient number of bubble tracks were recorded. At very low velocities there is some uncertainty regarding the accuracy of bubble velocity measurements in the vertical direction because there is a range of bubble diameters and, therefore, not all bubbles have exact neutral buoyancy. To determine flow patterns at very low velocities, more bubbles would need to be analyzed to get a statistically valid trend. Velocities were still found to be close to zero in most cases, as anemometer results had indicated earlier.

The results clearly indicated that the helium bubble generator method can be a useful technique for flow pattern visualization. It is a cost-effective technique when compared with laser based methods and gives the added advantage of providing information about velocity.

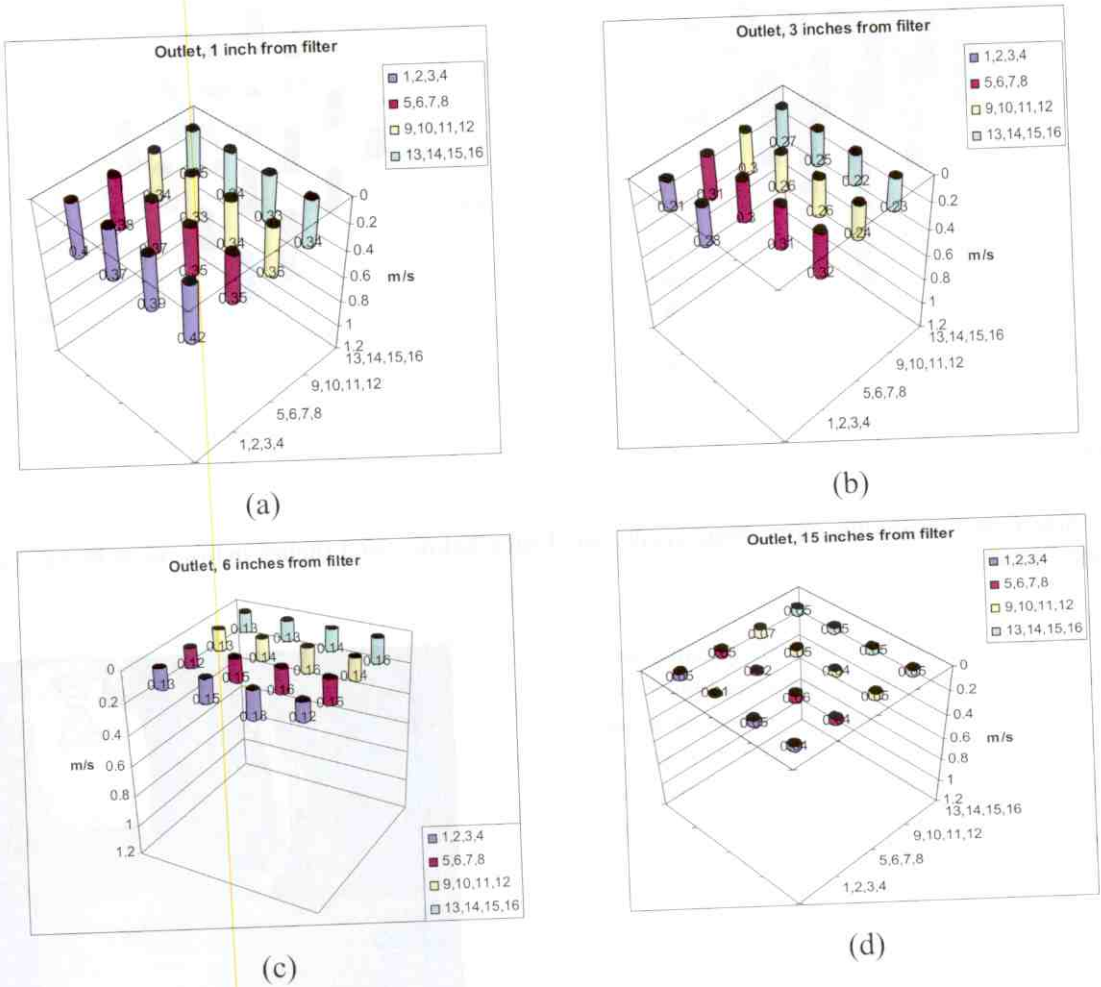


**Figure 14**

**Velocities below the return filter at various levels: (a) 1 inch below, (b) 3 inches below, (c) 6 inches below, and (d) 15 inches below.**

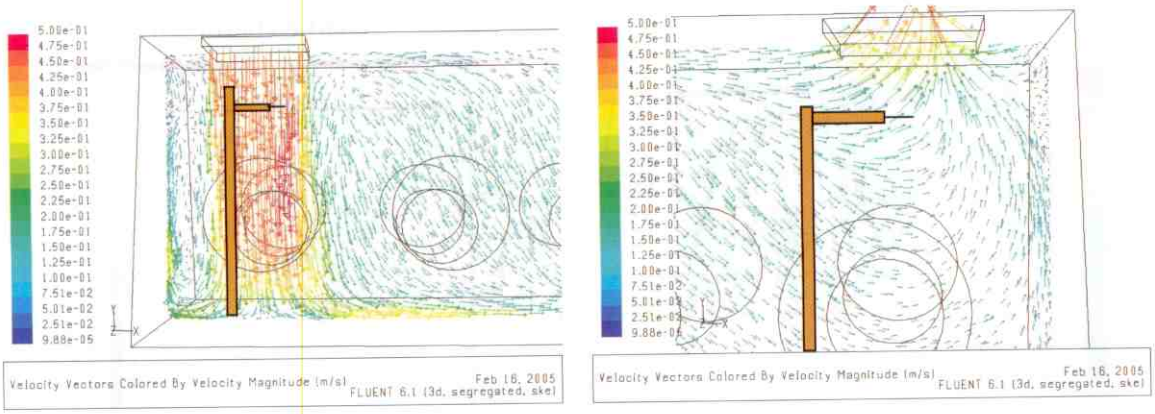


**Figure 15**

**Flow patterns near (a) supply, and (b) return sides with the probe superimposed.**

## 6 Discussion of Results

Good agreement between calculated and measured results was obtained for data collected at experimental conditions where measurement error was no more than 10%. Specifically, for the high pressure drop operating condition ($\Delta p$ = 1.3 inches of water) airflows are higher and the instrumentation is more accurate. At the nominal pressure drop (0.2 inches of water), comparisons between the calculated and measured velocities were less meaningful because in those areas of the isolator where the velocities were below 0.1 m/s anemometer measurement errors were greater than 20%, and not all helium bubbles were neutrally buoyant. However, in areas where the local velocities were higher and measurement errors are lower, such as a few inches below the inlet and outlet filters, measured and calculated values compared well.

When used within their measurement ranges, the hot wire anemometer and the helium bubble generator performed according to specifications. The anemometer provides a convenient method of measuring velocity magnitudes, but one must carefully orient the probe with respect to the prevailing flow field to ensure an accurate measurement. The helium bubble generator was less convenient but measured a specific flow vector. This facilitates a more direct verification of the CFD models. Additionally, a visual comparison can be made between the CFD-computed path and the path of the helium bubble. Both of these instruments performed best when the nominal flow velocity was greater than 0.45 m/s.

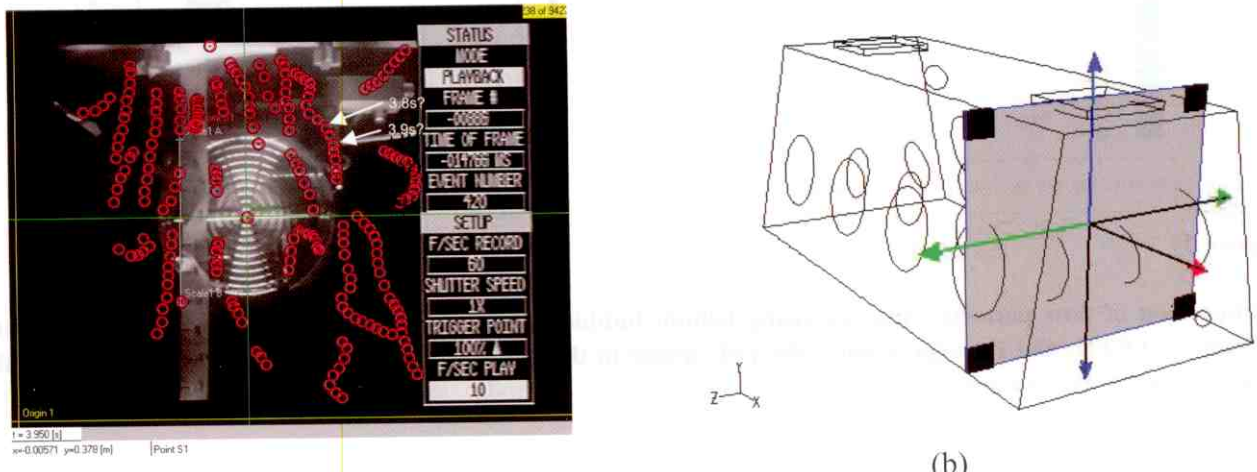


(a) (b)

**Figure 16**

**View of the (a) particle tracked in time, and (b) the plane for illumination and capture of bubbles.**

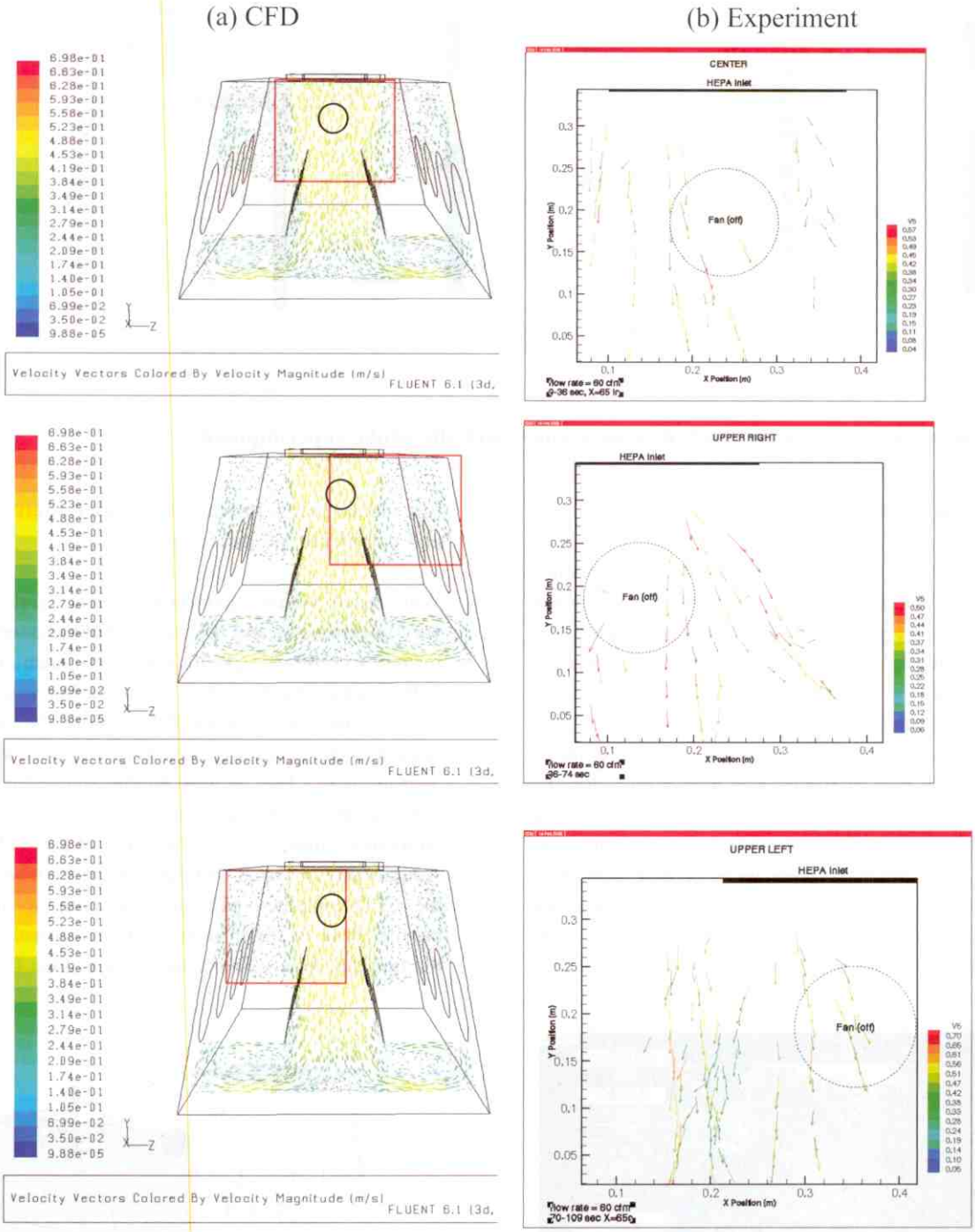


**Figure 17**

**Comparison of flow patterns obtained using helium bubble generator and CFD predictions at 0.45 m/s (60 ft$^3$/min): (a) CFD, and (b) experiment. The red square in the CFD plots corresponds to the region where the bubbles tracks were recorded.**

A suitable CFD model was constructed using less than one-half million cells. Above this level the solution was not sensitive to mesh size. RANS methods are suitable for modeling turbulence. Either the realizable K-ε or the K-ω method may be used. Because laminar, transition, and turbulent flow regimes exist in an isolator, the K-ω method is recommended. To obtain reasonable fidelity in the flow through the inlet and outlet

HEPA filters, a hexahedral mesh was required to ensure accurate computation of the filter pressure drop.

## 7 Conclusions

Airflow studies in a pharmaceutical isolator were performed successfully using the CFD models developed here. Comparisons of CFD predictions with air velocity measurements using a hot wire anemometer and a helium bubble generator gave good agreement. This validates our hypothesis that CFD modeling can predict gas and vapor flow vectors, and isolator pressures, with reasonable accuracy. These results are consistent with those from similar applications. Additionally, we have reported experiences with two measuring devices, an anemometer and a helium bubble generator, that can be used to verify CFD models, when such verification is necessary. Of course, verification experiments must be conducted in ranges where the devices give suitably accurate measurements.

This work demonstrates that CFD modeling is a powerful analysis tool for barrier systems and isolators. Because the CFD models are based on fundamental laws of fluid mechanics, a CFD model of an isolator is a kind of "computational lab" where a variety of "experiments" can be completed numerically before prototypes or production units are built or physical testing is performed. The CFD model allows for examination of the isolator in areas where placement of measuring devices is difficult or impossible. Further, from the computed flow velocities and pressure, one may evaluate design and operating conditions such as

- the placement of internal fans
- the effect on flow of the internals such as conveyors and star wheels
- the effect on flow of the presence or absence of containers
- the time to achieve a specified decontaminant concentration, as occurs in decontamination and aeration, as a function of location in the isolator
- the effect of placement of air/decontaminant supplies and returns (e.g., unidirectional *vs* non-unidirectional)
- the effect of number and size of air/decontaminant supplies and returns
- the placement of biological indicators for decontamination validation based on the presence of low velocity areas or recirculation zones

The advantages of making these kinds of assessments numerically using CFD are (1) reduced costs because fewer prototypes are constructed and less direct testing is required, and (2) enhanced fundamental understanding because the predictions are based upon fluid mechanics. These kinds of advantages should drive the use CFD into the mainstream of isolator design, validation, and operation.

## Acknowledgments

We acknowledge Birendra Kumar David of the Fluent Technical Support Center who gave useful advice on the modeling of porous media.

## References

1. Belly, S.; Wilkins, J. A technical review of isolators. *Pharmaceutical Engineering*, **1998,** *18* (2), 80–85.
2. Melgaard, H. L. Barrier isolator design issues. *Pharmaceutical Engineering*, **1994,** *14* (6), 24–30.
3. Nieskes, R. Isolators for Sterility Testing Workshop: Current Issues and Trends in Control Monitoring. *ISPE 2001 Washington Conference*, Arlington, VA, 2001.
4. FDA. *Pharmaceutical cGMPs for the 21st Century—A Risk-Based Approach*. http://www.fda.gov/cder/gmp/gmp2004/GMP_finalreport2004.htm, 2004.
5. FDA. *Guidance for Industry PAT—A Framework for Innovative Pharmaceutical Development, Manufacturing, and Quality Assurance*. http://www.fda.gov/cder/guidance/6419fnl.htm, 2004.
6. Johnson, R. W. *The Handbook of Fluid Dynamics*; CRC Press LLC: Boca Raton, FL, 1998; pp 2-12 to 2-15.
7. Kolesnikov, R.; Ryan, R.; Walters, D. B. Use of CFD to design containment systems for work with

hazardous materials. *Chemical Health and Safety,* **2004,** March/April, 17–20.

8. Kukura, J.; Campos Arratia, P.; Szalai, E. S.; Bittorf, K. J.; Muzzio, F. J. Understanding pharmaceutical flows. *Pharmaceutical Technology* **2002,** *72,* 48–72.

9. Wintner, B.; Divelbiss, J. Isolator evaluation using computer modeling. Part 1: Airflows within the mini environment. *Pharmaceutical Engineering* **2004,** *14,* 8–22.

10. Divelbiss, J.; Wintner, B. Isolator evaluation using computer modeling. Part 2: Hydrogen peroxide sterilization with two diluent fluids. *Pharmaceutical Engineering,* **1995,** *15* (3), 84–96.

11. Adams, D.; Brown, G. P.; Fritz, C.; Todd, T. R. Calibration of a near-infrared (NIR) $H_2O_2$ vapor monitor. *Pharmaceutical Engineering* **1998,** *18* (3), 1–11.

12. Bird, R. B.; Stewart, W. E.; Lightfoot, E. N. *Transport Phenomena*; John Wiley & Sons: New York, 1960, pp. 71–82 and pp. 153–161.

13. Johnson, R. W. *The Handbook of Fluid Dynamics;* CRC Press LLC: Boca Raton, FL, 1998; pp. 14–1 to 14–60.

14. Versteeg, H. K.; Malalasekera, W. *An Introduction to Computational Fluid Dynamics: The Finite Volume Method*; Addison-Wesley: Boston, MA, 1996.

15. Bell, B. Tubulent Flow Case Studies. *Fluent Users' Group Meeting 2003,* Manchester, NH, June 2003.

16. Wilcox, D. C. *Turbulence Modeling for CFD;* DCW Industries, Inc.: La Canada, CA, 1998.

17. Hinze, J. O. *Turbulence;* McGraw-Hill Publishing Co.: New York, 1975.

18. Fluent. *Fluent Users' Manual;* Fluent, Inc., Lebanon, NH, 2003.

19. Ferziger, J. H.; Perić, M. *Computational Methods for Fluid Dynamics,* 3rd ed.; Springer-Verlag: Berlin, Heidelberg, New York, 2002.

20. Anderson, J. D. *Computational Fluid Dynamics - the Basics with Applications*, McGraw-Hill: New York, 1995.

21. STERIS Corporation. *VHP 1000ED Biodecontamination System Operator Manual,* Erie, PA, 2002.

22. Fisher, J.; Caputo, R. Comparing and contrasting barrier isolator decontamination systems. *Pharmaceutical Technology,* **2004,** November, 68–82.

23. Klapes, N. A.; Vesley, D. Vapor-phase hydrogen peroxide as a surface decontaminant and sterilant. *Applied and Environmental Microbiology,* **1990,** *56* (2), 503–506.

24. Edwards, L. "Facility Design Considerations for Sterility Testing Isolators," *Barnett International Conference on Sterility Testing*, Washington, DC (May 2000).

25. Edwards, L. $H_2O_2$ gas decontamination cycle comparisons between rigid and flexible wall isolators. *la Calhène AUDITS 101 Conference*, Malvern, PA, October 2002.

26. Kanomax. *Kanomax Climomaster A533 Manual,* 2005.

27. Sage Action Inc. *SAI Bubble Generator Model 5 Console*, April 2002.

28. Eagleson Institute. *Testing HEPA Filters in Cleanrooms, HVAC Systems and Laminar Flow Equipment*, June 2004.

29. Zhao, L.; Zhang, Y.; Wang, X.; Riskowski, G. L.; Christianson, L. L. Measurement of Effect of Air Exchange Rate on Airflow Patterns in Ventilated Spaces Using Particle Image Velocimetry. *ASAE/CSAE Annual International Meeting, Toronto, ON,* 1999, pp 1–12.

30. Chan, V. S. S.; Delaure, Y. M. C.; Murray, D. B.; Fitzpatrick, J.A. Optical considerations for time-resolved digital PIV measurement in a single bubble flow against heated boundaries. *Measurement Science and Technology,* **2004,** *15,* N39–N42.